Surface Properties of Femtosecond Laser Ablated PMMA

Carmela De Marco,*,† Shane M. Eaton,‡ Raffaella Suriano,† Stefano Turri,† Marinella Levi,† Roberta Ramponi,‡,§ Giulio Cerullo,‡,§ and Roberto Osellame‡

Dipartimento di Chimica, Materiali e Ingegneria Chimica "Giulio Natta", Politecnico di Milano, Istituto di Fotonica e Nanotecnologie (IFN)-CNR, and Dipartimento di Fisica, Politecnico di Milano, Piazza Leonardo da Vinci 32, 20133 Milan, Italy

ABSTRACT The effects of femtosecond laser ablation on the physical and chemical properties at the surface of poly methylmethacrylate (PMMA) were studied. Femtosecond laser microfabrication caused the initially wetting behavior of PMMA to become nonwetting, mainly because of the laser-induced surface porosity at the submicroscale. Static and dynamic contact angle measurements along with morphological characterization revealed that after the laser irradiation, the system lies in an intermediate regime between those theorized by Wenzel and Cassie–Baxter. Spectroscopic analysis did not evidence any significant variation in the chemical properties of the processed polymeric surfaces.

KEYWORDS: femtosecond laser • ablation • wettability • polymer • PMMA • surface

INTRODUCTION

Microfluidic channels are used to manipulate small volumes of chemical and biological analytes for use in lab-on-chip (LoC) devices, which integrate the functionality of an entire biochemical laboratory on a single pocket-sized substrate (1, 2). Polymers are emerging as the materials of choice for disposable LoC devices because of their ease and low cost of manufacture, widely tunable properties, biocompatibility, and optical transparency. In the context of microfluidic channels, a crucially important characteristic of polymers is their surface wettability, which controls the flow behavior of biological reagents in microfluidic networks. Poly(methyl methacrylate) (PMMA) is an attractive substrate for microfluidics due to its moderate hydrophilicity (water contact angle, $\theta \approx 70°$), good optical transmission at visible and near-infrared wavelengths, and ability to be easily patterned by existing injection molding and hot embossing technologies.

Despite the great potential offered by LoC devices, their commercial exploitation has been slow thus far. One breakthrough that could promote the adoption of the LoC platform is a microfabrication technology with low-cost rapid prototyping capabilities. Rapid prototyping is an important stage in the production of LoC devices, enabling fast verification of designs without the need for microfludic simulations that do not always prove to be accurate. Although injection molding and hot embossing are attractive for mass production of microchannels, they are not suitable for rapid prototyping and cannot be used to alter the wettability properties of polymers for the realization of important microfluidic functions such as passive pumping, mixing, and switching.

To date, the most widely used technology for polymeric LoC rapid prototyping is micromilling (3), which is a rather well established technique, but the patterned microchannels suffer from limited resolution and surface quality because of the size of the milling tool. Laser ablation is another direct write rapid prototyping technique and has shown the ability to modify the wetting characteristics of microchannels (4, 5). Polymers linearly absorb laser radiation at ultraviolet and infrared wavelengths. Therefore, CO_2 ($\lambda = 10.6\,\mu$m) (4) and excimer ($\lambda = 193$, 248 nm) (5) lasers have commonly been applied to microfabrication of polymer microchannels, but they suffer from low spatial resolution and complex setups, respectively. In contrast, near-infrared photons ($\lambda = 800$ nm) from femtosecond lasers are nonlinearly absorbed in polymers through multiphoton absorption, enabling precise micromachining (6–11) and also the possibility to form diffraction gratings (12, 13) and optical waveguides (14–16) buried below the surface. The ultrashort laser pulses (<1 ps) offer further advantages of rapid energy deposition and fast ablation with minimal heat affected zone and a lower threshold for ablation compared to longer pulse sources (9, 17). Although femtosecond laser micromachining suffers from low throughput because it is a serial process, this hindrance becomes an important advantage for the localized and spatially selective tailoring of the surface wettability of a microchannel. The changes in surface chemistry and topography through laser ablation (4, 5) may be exploited to render a microchannel more hydrophilic or hydrophobic, depending on the application. In addition, femtosecond laser irradiation could be applied as a postprocessing step to locally tune the wettability of a microchannel fabricated by commercial mass production techniques.

A recent study (8) showed the possibility of altering the contact angle of PMMA by femtosecond laser irradiation;

* Corresponding author. E-mail: carmela.demarco@chem.polimi.it.
Received for review May 4, 2010 and accepted July 1, 2010
† Dipartimento di Chimica, Materiali e Ingegneria Chimica "Giulio Natta", Politecnico di Milano.
‡ Istituto di Fotonica e Nanotecnologie (IFN)-CNR.
§ Dipartimento di Fisica, Politecnico di Milano.
DOI: 10.1021/am100393e

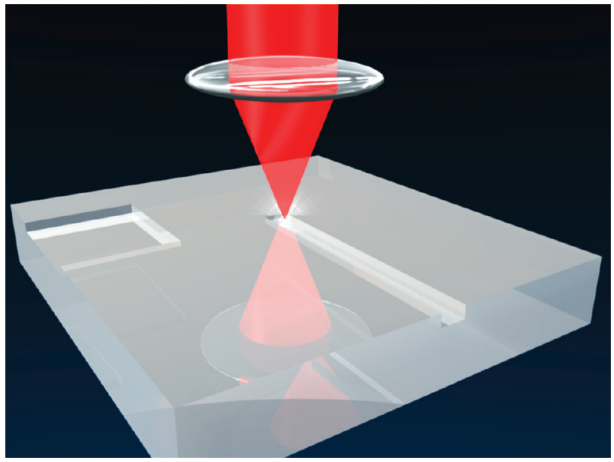

FIGURE 1. Diagram showing femtosecond laser micromachining method. Femtosecond laser pulses focused by a 100 mm focal length lens on the surface are used to ablate PMMA. Ablated features may be tailored using computer controlled motion stages.

however, only static contact angles were reported and the morphological contribution to the change in wettability was not accounted for. In this paper, we present a comprehensive characterization of the surface properties of femtosecond laser ablated PMMA. We show that the initially hydrophilic PMMA ($\theta = 74°$) becomes hydrophobic after laser ablation with a contact angle of approximately 100°, which in contrast with the results of reference (8) is nearly independent of laser fluence and suggests an intermediate regime between the well-known wetting theories by Wenzel (18) and Cassie−Baxter (19). Through dynamic contact angle measurements supported by microscopy and optical profilometry we show that surface morphology and roughness play a strong role on the resulting wettability, while spectroscopic analysis does not evidence any contribution to the change in contact angle from laser-altered surface chemistry. These results may pave the way for the implementation of a facile and low-cost method for spatially selective tuning of the wettability of polymeric materials.

EXPERIMENTAL METHODS

To ablate surface features in the polymer substrates, we applied a regeneratively amplified Ti:Sapphire laser (Integra-C FS-F, Quantronix) with 800 nm center wavelength, 1 mJ maximum pulse energy, $R = 1$ kHz repetition rate, and 150 fs pulse duration with a 100-mm focal length lens (spot size, $2w_0 = 20.4$ μm). The laser average power delivered to the sample was measured with a calibrated integrating sphere optometer after the focal plane of the focusing lens. As such, the measured laser power represents the actual power delivered to the sample despite the optical breakdown in air that was observed at the highest fluence. Figure 1 shows a diagram of how focused femtosecond laser pulses are used to ablate micrometer-scale features at the surface of a sample. Computer-controlled translation stages (M.511.DD, Physik Instrumente) were used to translate the sample to micromachine features with the desired geometry. The PMMA substrates (Shinkolite A L-#000) had dimensions of 3 mm ×50 mm ×50 mm. To remove debris after femtosecond laser irradiation, samples were rinsed with ultrapure water in an ultrasound bath for 15 min, and then dried in an oven at 40 °C for 30 min.

After laser ablation, an optical microscope was used to assess the morphology of the surface structures. The surface roughness was estimated by a laser profilometer (UBM-Microfocus Compact) with a vertical resolution of 60 nm and a lateral resolution of 1 μm. To obtain more accurate characterization of the topography of the irradiated surfaces, scanning electron microscopy (SEM), EVO 50 extended pressure (ZEISS) was employed. Infrared spectra of polymers before and after laser irradiation were acquired using a Perkin-Elmer Spectrum 2000 FTIR spectrometer in attenuated total reflectance (ATR) mode using a Si microcrystal tip with a contact diameter of 100 μm. Spectra were collected from 700 to 4000 cm^{-1}. All the output spectra are the result of the combination of 32 sequential scans for noise reduction. X-ray photoelectron spectroscopy (XPS) was carried out to gain further insight into surface chemistry changes induced by laser treatment of PMMA. Measurements were carried out with a PHI 5600 ci ESCA system (Al kα source, power 250 W, voltage 14 kV). The instrument calibration was done setting the binding energy of Au 4f, Ag 3d, and Cu 2p at 84.0, 368.3, and 932.6 eV, respectively. The spectra were aligned setting the binding energy of C1s at 285.0 eV. Both low-resolution survey analyses and high-resolution analyses on carbon and oxygen peaks were carried out.

The contact-angle measurements were performed using an optical video contact angle system (OCA-15-plus, Dataphysics). A 1 μL droplet of water (Chromasolv water for HPLC, Sigma Aldrich), having a surface tension of 78.2 mN/m, was dispensed on the samples using the electronic syringe unit of the instrument equipped with a 500-μL Hamilton syringe. The static contact angle was measured using the sessile drop method with dedicated software (SCA 2.0) determining the contact angle based on the Young−Laplace fitting. The dynamic contact angle was measured using the needle in sessile drop method, dispensing and removing 3 μL of water at a rate of 1 μL/s, for 5 cycles, with a delay time of 1 s. For benchmarking purposes, we also processed polymer samples with a micromilling machine (Charlyrobot SAS).

RESULTS AND DISCUSSION

We first assessed the potential of femtosecond laser micromachining for the rapid prototyping of microfluidic channels on the surface of polymer substrates. We fabricated rectangular cross-section microchannels by performing multiple parallel scans at a single depth and separated laterally by 4 μm. The produced microchannels were of very good quality with sharp edges and low roughness as shown in the SEM image in Figure 2a. The channel width can be easily tailored by defining the appropriate number of parallel scans, while its depth is strongly dependent on the laser fluence and can thus be easily controlled. Figure 2b shows the depth versus fluence data together with a logarithmic fit, according to (7) $y = A\log(Bx)$, where A and B are fitting parameters. The x-intercept of the fitting curve ($1/B$) yields a threshold fluence of $F_{th} = 0.85$ J/cm^2. A scan speed of $v = 1$ mm/s was applied to fabricate the microchannels so that the number of pulses overlapped within the spot size diameter during the scan was $N = 2w_0R/v = 20$. Therefore, incubation will reduce the damage threshold with respect to single pulse ablation (9−11). Baudach et al. found that the threshold fluence for multipulse ablation was well-represented by $F_{th}(N) = F_{th}(1)N^{\xi-1}$, where $F_{th}(N)$ is the ablation threshold fluence for N pulses and ξ is the degree of incubation (10). According to this formula, using the parameters $\xi = 0.67$, $F_{th}(1) = 2.6$ J/cm^2 determined by Baudach et al., the threshold fluence in PMMA for $N = 20$ is predicted

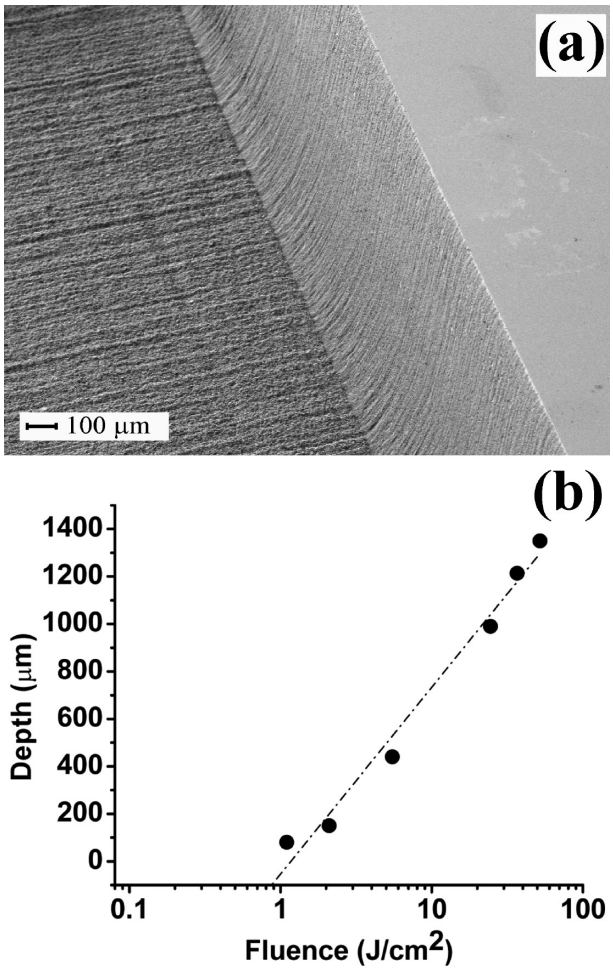

FIGURE 2. (a) SEM image of ablated microchannel produced in PMMA. (b) Ablated depth versus incident laser fluence. Experimental data points are well represented by a logarithmic response (dashed line). The *x*-intercept of the fitted logarithmic reveals a threshold fluence of 0.85 J/cm^2 ($N = 20$ pulses per spot).

to be 0.97 J/cm^2, which is in good agreement with the value of 0.85 J/cm^2 obtained in our study.

To study the wettability and surface roughness of femtosecond laser ablated microchannels in polymers, it is necessary to have a sufficiently large area to accommodate the drop of liquid and to easily perform optical profilometry. The multiscan writing method described above was applied to ablate a square of dimensions 4 mm × 4 mm. In the first wettability experiments, it was observed that the multiscan technique (notwithstanding the high overlap between subsequent scans) induced the formation of nonisotropic droplets, with a preferential spreading along the scan direction. To reduce the dependence of the surface roughness on the scan direction (Figure 3a), the squares were fabricated in two steps using a grid pattern (Figure 3c). First, a square was fabricated by 1000 scans along the *y*-axis with 4-μm transverse separation between scans. Then, a second square was written directly over the first square with the same focusing condition. However, this time the scans were performed along the *x*-axis. As shown by optical microscope image in Figure 3b, this grid scanning method gives rise to an ablated square with a more randomized roughness allowing for accurate and isotropic contact angle measurements. In

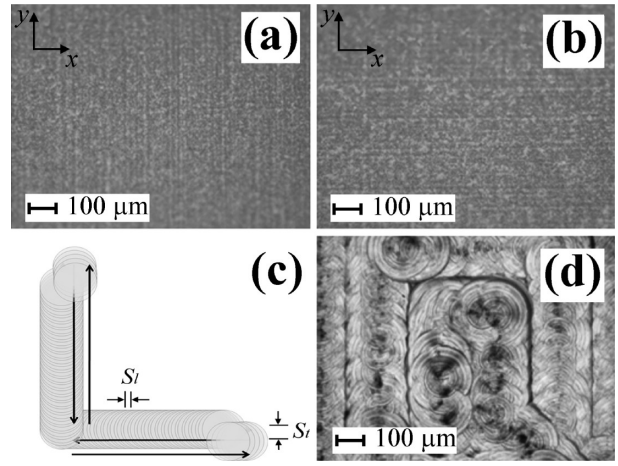

FIGURE 3. Overhead microscope image of ablated squares in PMMA scanned along (a) *y* axis and (b) both *x* and *y* axes as shown in (c) with transverse separation $s_t = 4$ μm between scans and longitudinal separation of $s_l = 1$ μm, defined by the 1 mm/s scan speed and 1 kHz repetition rate. (d) Microscope image of micromilled area in PMMA showing a morphology influenced by the tool geometry, which gives rise to increased roughness compared to femtosecond laser ablation.

Figure 3d, an area machined by micromilling is shown for comparison, with the milling traces produced by the tool giving rise to a rougher topography than the areas machined by femtosecond laser ablation.

For a quantification of the surface roughness, Figure 4 shows an optical profilometer scan of the surface topography as a function of incident laser fluence. As the fluence is increased, one clearly sees an increase in roughness. For all fluences, the roughness appears to be random without significant directionality, which could influence the contact-angle measurement.

Table 1 shows the roughness values from the profilometer measurements (Figure 4) and the ablation depth as a function of average laser fluence. For comparison, the last line reports the roughness and depth corresponding to the micromilled sample. As expected, both the depth and average roughness increase with laser fluence. Although an increased roughness cannot be considered a positive feature in the fabrication of microfluidic channels, it should be underlined that by comparing the roughness of a laser formed channel with a depth comparable (150 μm) to the micromilled channel (201 μm), a markedly lower roughness for the higher-precision femtosecond laser technology is evident.

To investigate the effects of femtosecond-laser irradiation on wettability, static and dynamic contact angle measurements were carried out before and after the laser processing. The contact angle value on pristine PMMA was measured to be 74.1° ± 1.3°, the same reported in literature (20). PMMA samples were washed in water after laser exposure to remove the residual PMMA debris created during the laser irradiation. As shown in Figure 5, PMMA debris strongly affects the contact-angle results leading to an apparent effect of hydrophilization of the substrate (contact angle ~20°, Figure 5a). The true hydrophobic behavior of the laser-processed area is revealed after rinsing and drying the

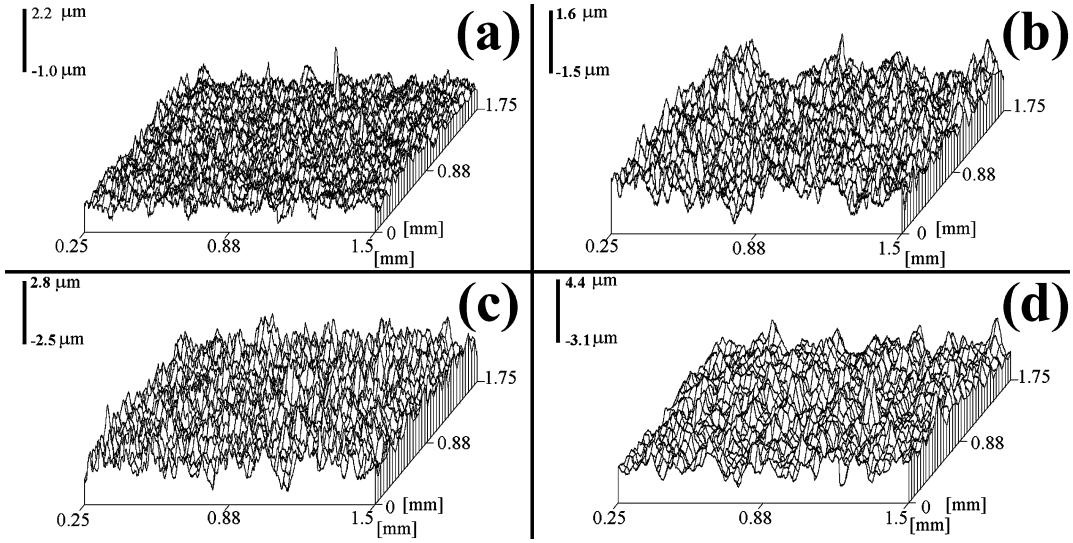

FIGURE 4. Optical profilometer scan of ablated surface over 1.25 mm ×1.75 mm area of laser ablated area for fluences of (a) 1.1, (b) 2.1, (c) 5.5, and (d) 52.0 J/cm^2.

Table 1. Average Roughness, Root Mean Square Roughness, and Depth of Areas Ablated in PMMA As a Function of Laser Fluence (last row shows the roughness values for a micromilled volume)

fluence (J/cm^2)	avg roughness, R_a (nm)	rms roughness, R_q(nm)	depth (μm)
0	11	17	0
1.1	224	303	80
2.1	365	464	150
5.5	508	645	440
52.0	626	785	1340
micromilling	649	1307	201

processed sample, showing a contact angle which increased to 94° (Figure 5b). The presence of the debris is also evident observing at the optical microscope the ablated surfaces before (Figure 5c) and after (Figure 5d) washing.

Changes in the observed surface wettability may be due to roughness effects and/or to modification of surface chemistry. Two different theories were developed to explain the effect of surface roughness on wettability. The first one is described by the Wenzel equation (18):

$$\cos\theta_W = r\cos\theta_Y$$

where θ_W is the actual contact angle on a real rough surface or Wenzel's angle, r is the ratio of the actual area of the solid surface to its nominal area, and θ_Y is the equilibrium Young contact angle observed on ideally smooth surface. Because r is always greater than 1, this model predicts an enhanced hydrophilicity ($\theta_W < \theta_Y$) for hydrophilic surfaces ($\theta_Y < 90°$), and an enhanced hydrophobicity ($\theta_W > \theta_Y$) for hydrophobic surfaces ($\theta_Y > 90°$). This model takes into account a complete wetting of droplet with the underneath substrate. The second theory was derived by Cassie and Baxter (19, 21) and assumes that the liquid does not completely wet the roughened substrate. The proposed expression for describing this situation is given by the following equation (21)

$$\cos\theta_{CB} = r_f f\cos\theta_Y + f - 1$$

where θ_{CB} is the Cassie–Baxter contact angle, f is the fraction of the solid surface in contact with the liquid, and r_f is the surface ratio of the wet area to its nominal area. When $f = 1$ and $r_f \equiv r$, the Cassie–Baxter equation becomes the Wenzel equation. Because f and r_f are always less than 1, the Cassie–Baxter model predicts that roughening a surface always increases the contact angle. The Cassie–Baxter model is appropriate for describing surfaces that are largely heterogeneous, as is the case of polymeric materials. If a surface is rough enough so that air may be entrapped between the liquid and the solid, the interface becomes composite and the contact angle increases with roughness even if the surface chemistry is intrinsically hydrophilic. Figure 6 shows the static contact angle on PMMA samples irradiated at fluences of 1.1, 2.1, 5.5, 24.5, 36.7, and 52.0 J/cm^2, revealing a nearly constant hydrophobic behavior for all the different fluences employed, in contrast with results previously reported (8), which show a dependence of the wettability on the laser fluence employed. We believe that the difference between our results and those reported in reference (8). can be attributed to the following two reasons: (i) the lower roughness of the ablated areas in our case, which we found to influence CA measurements; (ii) the cleaning procedure that we performed after ablation, removing debris, which we found to result in an artificially enhanced surface hydrophilicity (see Figure 5).

The results presented in Figure 6, showing a static contact angle nearly independent of laser fluence, are not consistent with Wenzel's model, according to which contact angle should decrease with increasing roughness, i.e., increasing laser fluence. This actual behavior can be explained assuming that air pockets, trapped between water and the PMMA

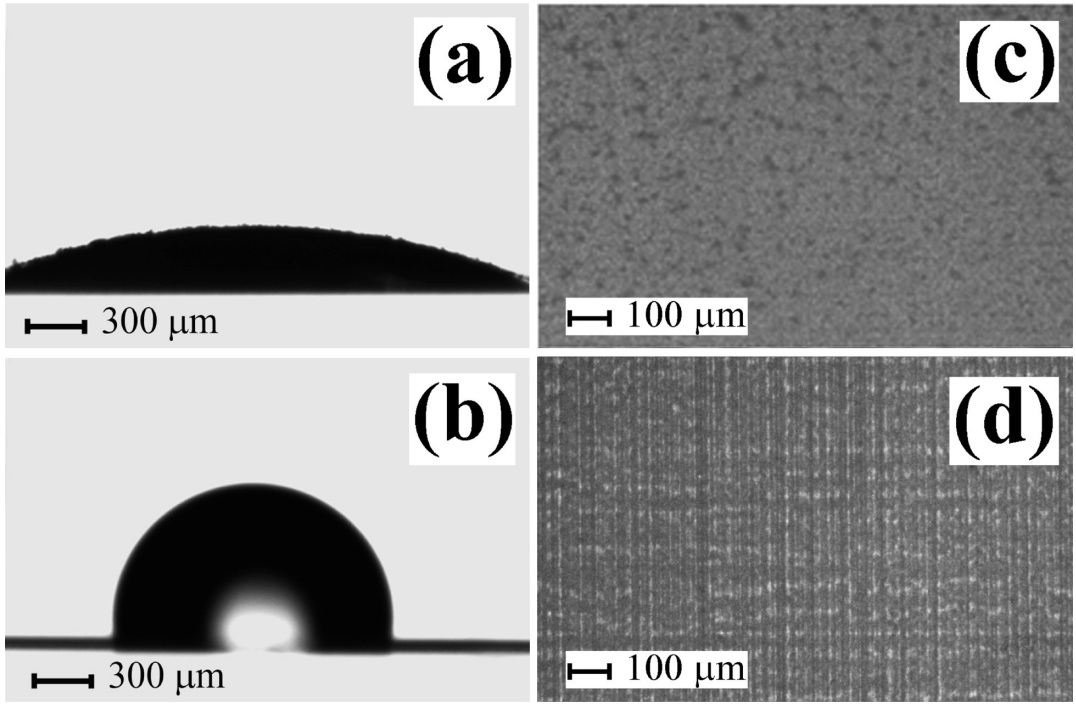

FIGURE 5. Photographs of a water droplet on a PMMA sample on a laser ablated area irradiated with 3.1 J/cm^2 for the case of: (a) no rinsing where the debris caused a decreased contact angle and (b) rinsing in water, which showed an increased contact angle and hydrophobic behavior. Optical images of the same PMMA sample (c) before and (d) after washing.

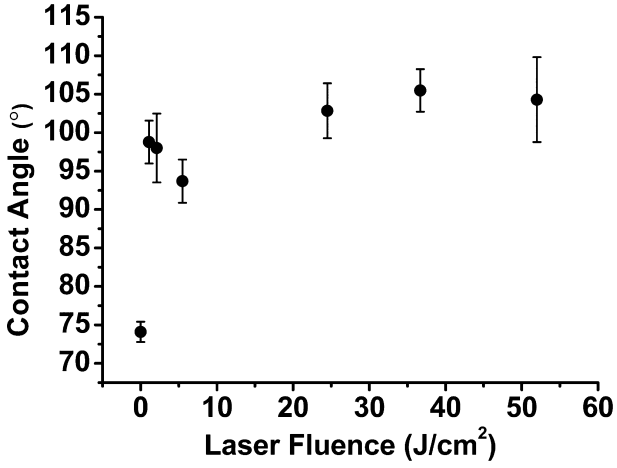

FIGURE 6. Static water contact angle on pristine PMMA (at 0 J/cm^2) and irradiated PMMA versus laser fluence.

substrate below, prevent a complete wetting of the substrate. This hypothesis is supported by the SEM images shown in Figure 7, which give better insight into surface morphology of the substrate, characterized by an evident superficial porosity. The dimension of the pores does not appear to change significantly despite the 50-fold increase in laser fluence, confirming that the contact-angle measurements depend mostly on surface texture rather than on roughness.

Instead, the surface roughness induced by the ablation may be responsible for the standard deviation of static contact-angle measurements observed in Figure 6, for which the system may lie in one of the many metastable states allowed. To better investigate the metastable states induced by laser irradiation at the solid/liquid interface, dynamic contact angle measurements were carried out to evaluate

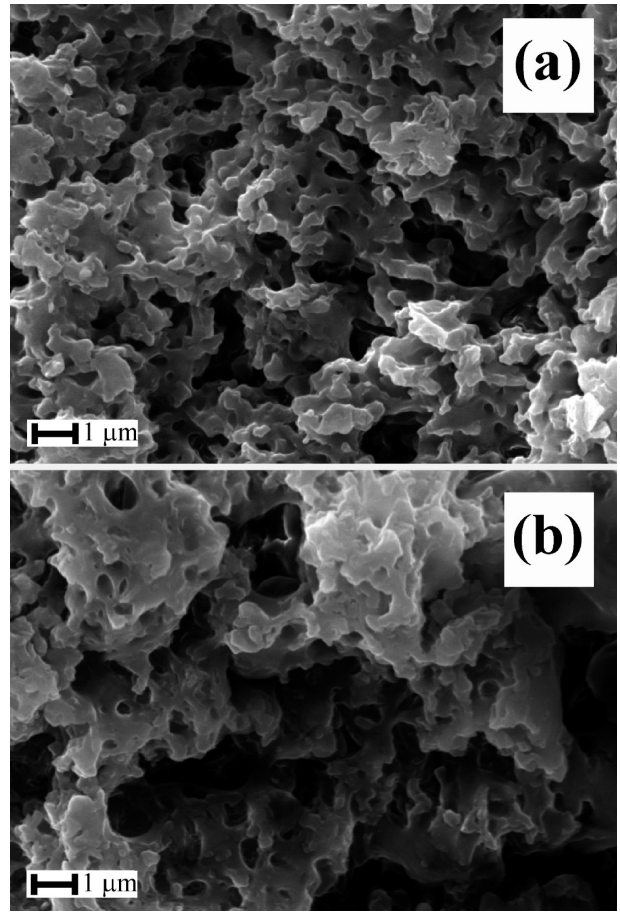

FIGURE 7. Magnified SEM images of laser ablated areas for fluences of (a) 1.1 J/cm^2 and (b) 52.0 J/cm^2 showing porous surfaces.

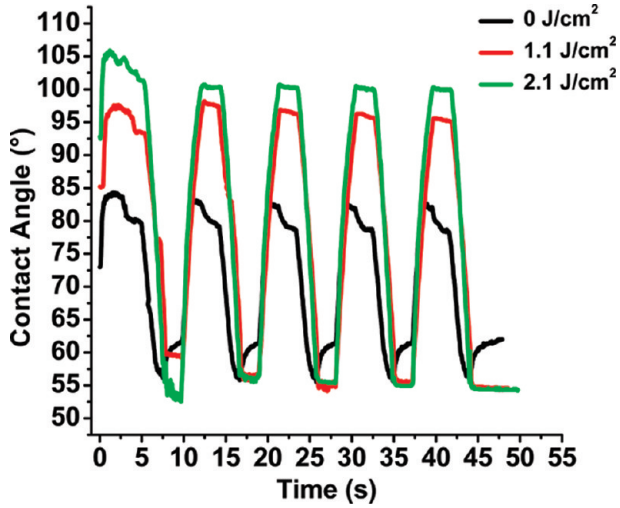

FIGURE 8. Receding and advancing contact angles and the relative hysteresis at different ablation fluences.

the receding angle (θ_r), the advancing angle (θ_a) and the difference $\Delta\theta$ between θ_a and θ_r, which is referred to as contact angle hysteresis. Figure 8 shows the values of θ_r, θ_a, and $\Delta\theta$ for pristine PMMA (0 J/cm^2) and for two ablation fluences (1.1 and 2.1 J/cm^2).

It can be observed that θ_r has the same value on pristine and on laser-ablated PMMA, whereas θ_a increases with fluence, i.e., with increasing roughness. As reported in literature (5, 22, 23), contact angle hysteresis is predicted to decrease with increasing roughness for surfaces that follow a Cassie–Baxter's model. The fact that we observe an increased hysteresis may be explained assuming that our ablated surfaces, showing a nonuniform porosity (Figure 7), are in an intermediate state between Wenzel and Cassie–Baxter, a state observed in previous studies on surfaces with a nonhomogenous topography (24, 25), and recently obtained on PMMA using laser irradiation (26).

As reported in the literature (27), the air pockets formed between the droplet and the substrate are metastable and if an external pressure is applied, the liquid can fill the pores, and the surface behaves as in a Wenzel state. In our case, the external pressure could be given by increasing the droplet volume during the dynamic measurements. During static contact angle measurements, the Cassie–Baxter state dominates. However, the wetting behavior changes when the droplet expands in volume in dynamic contact angle measurements. In this case, the liquid droplet fills the pores of the roughened substrate, and the Wenzel state becomes dominant. This suggests that the energy barrier between the Cassie–Baxter state and the third intermediate state is low. Moreover, the fact that receding angles are associated with the high-surface-energy regions and do not change after laser irradiation (Figure 8) suggests that the increased hysteresis is caused mainly by geometrical effects (increased roughness and induced microporosity) and that no significant modification in polymer surface chemistry occurs.

To quantitatively assess the issue of surface chemistry changes, we carried out the C 1s and O 1s XPS analysis of the pristine PMMA sample (0 J/cm^2), and the two samples

Table 2. Atomic Percentage of Carbon and Oxygen and Relative Ratio, For Pristine PMMA and PMMA Ablated at Minimum and Maximum Fluence

fluence (J/cm^2)	C (at %)	O (at %)	C/O
0	72.2	27.2	2.6
1.1	70.5	29.4	2.4
52.0	70.2	28.1	2.5

irradiated at the minimum (1.1 J/cm^2) and maximum (52.0 J/cm^2) irradiation fluence. The atomic abundance of carbon and oxygen and their relative ratio for each sample were measured and reported in Table 2. We can observe that carbon to oxygen ratio for each tested fluence remains nearly equal to the theoretical stoichiometric carbon to oxygen ratio of the PMMA (C/O = 2.5).

The high resolution XPS spectra of C 1s (Figure 9a) and O 1s (Figure 9b) do not reveal significant variations in the peak intensities and peak positions. The XPS binding energies and the relative group assignments for pristine PMMA are compared to literature values in Table 3.

The main difference in the spectra is a slight broadening of the peak linewidths with increasing fluence. In particular,

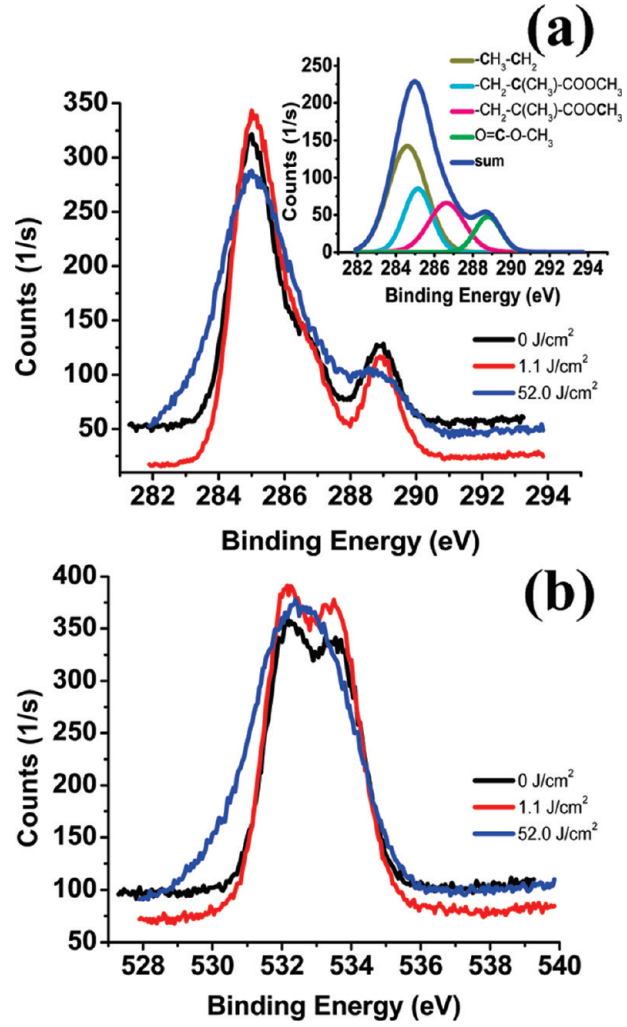

FIGURE 9. (a) Carbon XPS spectra and (b) oxygen XPS spectra of pristine PMMA (black line) and PMMA irradiated at the minimum (red line) and maximum (blue line) fluence. Inset: deconvoluted C1s XPS spectra of PMMA irradiated at maximum fluence.

Table 3. Comparison between XPS Binding Energies and Relative Group Assignments for Our Pristine PMMA and Those Reported in Literature

	binding energy (eV)		
atom	from literature (28)	our PMMA	group type
C 1s	285.00	284.80	$-\mathbf{C}H_3$, $-\mathbf{C}H_2$
	285.72	285.42	$-CH_2-\mathbf{C}(CH_3)-COOCH_3$
	286.79	286.61	$-CH_2-C(CH_3)-COO\mathbf{C}H_3$
	289.03	288.89	$O=\mathbf{C}-O-CH_3$
O 1s	532.40	532.11	$-C=\mathbf{O}$
	533.90	533.64	$-\mathbf{O}-CH_3$

the O 1s XPS spectrum changes from having two peaks in the pristine PMMA (Figure 10a) to a single broader peak in the PMMA irradiated at the maximum fluence (Figure 10b). The increased linewidths, which cause a merging of the two peaks, may be ascribed to a wider electron scattering from a more roughened surface, whereas the binding energies corresponding to the C−O and C═O bonds are the same for the two investigated samples, as demonstrated by the deconvolution curves of the spectra (Figure 10). However, some alterations of chemical groups after irradiation at high laser fluences cannot be excluded.

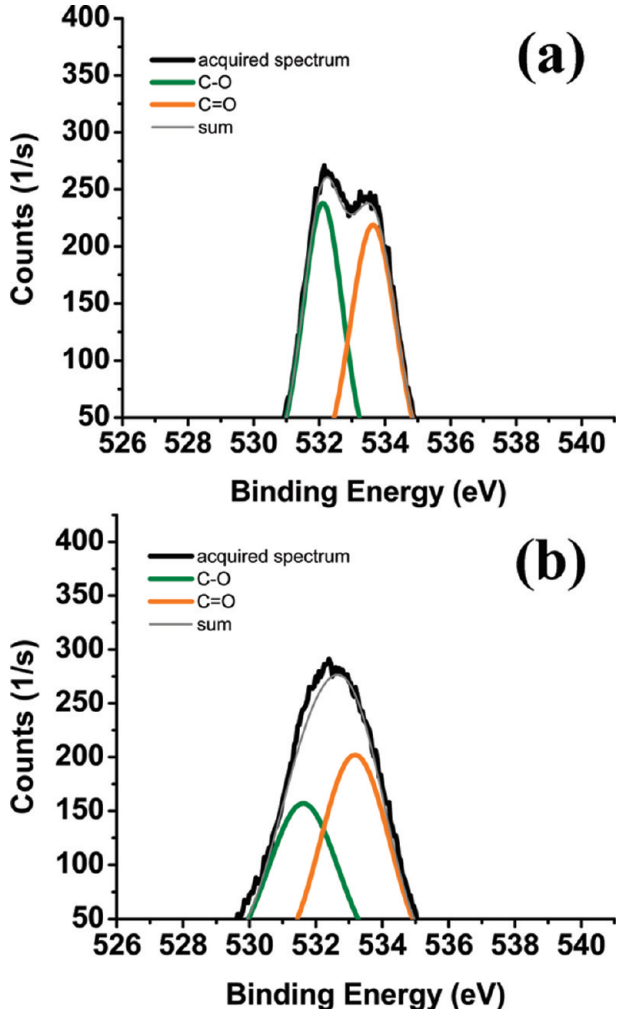

FIGURE 10. Deconvoluted oxygen XPS spectra of (a) pristine PMMA and (b) PMMA irradiated at 52.0 J/cm^2.

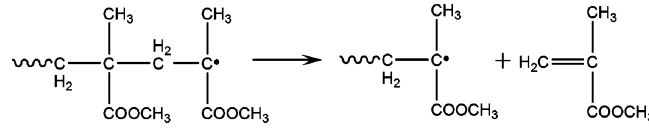

FIGURE 11. Scheme of the laser-induced depolymerization of one repetition unit out of the PMMA backbone.

Recent studies (8) on chemical changes induced on PMMA substrate by femtosecond-laser irradiation revealed that chemical modifications to PMMA were possible with sufficiently high fluence. An increased oxygen content was found for high fluences, supported by the generation of methane and carbon oxide as the degradation products of the free methyl formate radical. In contrast, XPS data for the experiments of the present work showed a remarkably constant value of the C/O stoichiometric ratio, always close to the theoretical value (see Table 2). As a matter of fact any degradation mechanism involving a side groups bond breaking (elimination of $\bullet CH_3$ or $\bullet OCH_3$ radicals, formation of formates of the type $-CH_2CH(CH_3)CHO$, decarbonylation with loss of CO or CO_2) would involve a significant change of the C/O stoichiometric ratio, which is not our case. On the other hand a random bond breaking in the main chain would lead to the formation of macroradicals of the type $CH_2^{\bullet}C(CH_3)COOCH_3-$, which are not stable but in case of PMMA tend to evolve to lower molecular weight fragments and especially monomer through the well-known unzipping mechanism (29). This nonoxidative mechanism, a scheme of which is shown in Figure 11, can be represented as the reverse of polymerization and in our case could be an explanation of the good optical quality retained by PMMA during the ablation process, which is beneficial for the development of optofluidic devices.

It is important to point out that, in agreement with cited studies (8, 30), we also observe that the peaks corresponding to the C−O and C═O merge for the sample ablated at maximum fluence. This behavior was attributed to the formation of formates (30), but because in our case the atomic C/O ratio does not vary with irradiation fluence, we believe that it is mainly an effect related to the morphology of the substrate, since the roughness of the substrate may affect the XPS data (31, 32).

To confirm the chemical analysis performed by XPS and give some information also on the state of possible degradation of the polymer in the areas surrounding the ablated zone, infrared spectra of PMMA at the ablation site were acquired in ATR mode. The sampling depth of polymer surfaces by this spectroscopy analysis (about 1.5 μm at 1000 cm^{-1}) is much greater than that by XPS (∼1−10 nm). Therefore, the latter analyzes a depth of about one monolayer at the surface of materials, whereas the former technique is capable of a deeper sample analysis.

As shown in Figure 12, there is no difference between the infrared spectrum of the ablated and the pristine PMMA. To evaluate the presence of any oxidative degradation process, we take into account the carbonyl index, which is the ratio between the maximum absorptions due to the carbonyl groups stretching (at 1720 cm^{-1}) and that due to

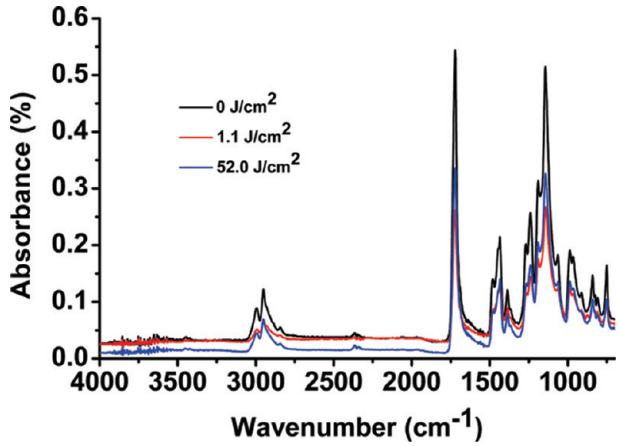

FIGURE 12. ATR infrared spectra of pristine PMMA (black line) and PMMA ablated at 1.1 J/cm^2 (red line) and 52.0 J/cm^2 (blue line).

the alkyl groups stretching (at 2950 cm^{-1}). Again, no significant change can be observed between carbonyl index of pristine sample ($A_{C=O/C-H} = 5.10$) and that of the laser-ablated sample ($A_{C=O/C-H} = 5.14$). This can be a further confirmation of prevailing nonoxidative degradation of the polymer through unzipping.

CONCLUSIONS

In this work, we have presented a systematic and comprehensive study of the surface properties of PMMA following femtosecond laser ablation. In summary, femtosecond laser ablation was found to alter the wettability of PMMA. In particular, the PMMA wetting behavior switches from moderately hydrophilic to hydrophobic after laser ablation, independent of the above-threshold laser fluence. We observed that the changed wettability is mainly a consequence of the porous morphology induced at the submicroscale after the laser processing, and that an intermediate state between those described by Wenzel and Cassie−Baxter occurs. The chemistry of the polymeric substrates was not altered after the laser irradiation, as confirmed by spectroscopic analysis.

Femtosecond laser ablation appears as a versatile technique for rapid prototyping of microfluidic devices, guaranteeing lower surface roughness with respect to micromilling while preserving the sample optical quality. Further, this technique could be applied to tailor the wettability of the substrate surface with micrometer spatial resolution, enabling the implementation of more microfluidic functionalities.

Acknowledgment. This work was supported by the European Commission, FP7 Project Contract No. ICT-2007-224205 (microFLUID - micro-Fabrication of polymeric Lab-on-a-chip by Ultrafast lasers with Integrated optical Detection). The authors thank the Institut für Mikrotechnik Mainz (IMM), Germany, for providing micromilled PMMA samples.

REFERENCES AND NOTES

(1) Whitesides, G. M. *Nature* **2006**, *442*, 368–373.
(2) Reyes, D. R.; Iossifidis, D.; Auroux, P.-A.; Manz, A. *Anal. Chem.* **2002**, *74*, 2623–2636.
(3) Friedrich, C. R.; Vasile, M. J. *Microsyst. Technol.* **1996**, *2*, 144–148.
(4) Waugh, D. G.; Lawrence, J.; Morgan, D. J.; Thomas, C. L. *Mater. Sci. Eng., C* **2009**, *29*, 2514–2524.
(5) Qi, H.; Chen, T.; Yao, L.; Zuo, T. *Microfluid. Nanofluid.* **2008**, *5*, 139–143.
(6) Serafetinides, A. A.; Makropoulou, M.; Fabrikesi, E.; Spyratou, E.; Bacharis, C.; Thomson, R. R.; Kar, A. K. *Appl. Phys. A: Mater. Sci. Process.* **2008**, *93*, 111–116.
(7) Lee, A. J.; Dawes, J. M.; Withford, M. J. *J. Laser. Appl.* **2008**, *20*, 154–159.
(8) Wang, Z. K.; Zheng, H. Y.; Lim, C. P.; Lam, Y. C. *Appl. Phys. Lett.* **2009**, *95*, 111110–3.
(9) Krüger, J.; Kautek, W. *Adv. Polym. Sci.* **2004**, *168*, 247–289.
(10) Baudach, S.; Bonse, J.; Krüger, J.; Kautek, W. *Appl. Surf. Sci.* **2000**, *154−155*, 155–560.
(11) Klinger, D.; Sobierajski, R.; Nietubyć, R.; Krzywiński; Pełka, J.; Juha, L.; Jurek, M.; Żymierska, D.; Guizard, S.; Merdji, H. *Radiat. Phys. Chem.* **2009**, *78*, S71–S74.
(12) Kallepalli, D. L. N.; Rao Desai, N.; Rao Soma, V. *Appl. Opt.* **2010**, *49*, 2475–2489.
(13) Baum, A.; Scully, P. J.; Perrie, W.; Jones, D.; Issac, R.; Jaroszynski, D. A. *Opt. Lett.* **2008**, *33*, 651–653.
(14) Gattass, R. R.; Mazur, E. *Nat. Photon.* **2008**, *2*, 219–225.
(15) Sowa, S.; Watanabe, W.; Tamaki, T.; Nishii, J.; Itoh, K. *Opt. Express* **2006**, *14*, 291–297.
(16) Baum, A.; Scully, P. J.; Basanta, M.; Paul Thomos, C. L.; Fielden, P. R.; Goddard, N. J.; Perrie, W.; Chalker, P. R. *Opt. Lett.* **2007**, *32*, 190–192.
(17) Joglekar, A. P.; Liu, H.-h.; Meyhofer, E.; Mourou, G.; Hunt, A. J. *P. N. Acad. Sci. USA* **2004**, *101*, 5856–5861.
(18) Wenzel, R. N. *J. Phys. Chem.* **1949**, *53*, 1466–1467.
(19) Cassie, A. B. D.; Baxter, S. *Trans. Faraday Soc.* **1944**, 546–551.
(20) Dann, J. R. *J. Colloid Interface Sci.* **1970**, *32*, 302–321.
(21) Marmur, A. *Langmuir* **2003**, *19*, 8343–8348.
(22) Quéré, D. *Physica A* **2002**, *313*, 32–46.
(23) Baldacchini, T.; Carey, J. E.; Zhou, M.; Mazur, E. *Langmuir* **2006**, *22*, 4917–4919.
(24) Seung-Mo, L.; Tai Hun, K. *J.Micromech. Microeng.* **2007**, *17*, 687.
(25) Gao, L.; McCarthy, T. J. *Langmuir* **2007**, *23*, 3762–3765.
(26) Waugh, D. G.; Lawrence, J.; Walton, C. D.; Zakaria, R. B. *Opt. Laser Technol.* **2010**, *42*, 347–356.
(27) Lafuma, A.; Quere, D. *Nat. Mater.* **2003**, *2*, 457–460.
(28) Kaczmarek, H.; Chaberska, H. *Appl. Surf. Sci.* **2009**, *255*, 6729–6735.
(29) Grassie, N., *Chemistry of High Polymer Degradation Processes*; Butterworths Scientific Publication: London, 1956.
(30) Wochnowski, C.; Metev, S.; Sepold, G. *Appl. Surf. Sci.* **2000**, 706–711.
(31) Olive, G. *Surf. Sci.* **1993**, *297*, 83–90.
(32) Gunter, P. L. J.; Niemantsverdriet, J. W. *Appl. Surf. Sci.* **1995**, *89*, 69–76.

AM100393E